Heliyon 10 (2024) e38794

Contents lists available at ScienceDirect

Heliyon

journal homepage: www.cell.com/heliyon

Research article

Novel electrochemical sensor based on poly($[Cu(H_2O)_2P_2]I_2$)/GCE for the determination of trimethoprim in clinical samples and cow's milk samples

Melaku Metto [a,b,*], Alemu Tesfaye [a], Minaleshewa Atlabachew [a,c], Atakilt Abebe [a]

[a] Department of Chemistry, College of Science, Bahir Dar University, Ethiopia
[b] Department of Chemistry, College of Natural and Computational Sciences, Injibara University, Ethiopia
[c] Department of Chemistry, College of Natural and Computational Sciences, Debark University, Ethiopia

ARTICLE INFO

Keywords:
Trimethoprim
Electrode fabrication
Diaquabis(1,10-phenanthroline copper (II) iodide
Square wave voltammetry
Real samples

ABSTRACT

A Novel bioanalytical detector based on Poly(Diaquabis(1,10-phenanthroline copper (II) Iodide) (poly($[Cu(H_2O)_2P_2]I_2$)/GCE) has been fabricated by potentiodynamic polymerization of [Cu $(H_2O)_2P_2]I_2$. The synthesized complex and the fabricated electrodes showed a promising electrocatalytic behavior towards the electrooxidation of Trimethoprim (TPM). Based on the regression coefficient value of scan rate with peak current and square root of peak current, the oxidation of TMP at poly($[Cu(H_2O)_2P_2]I_2$)/GCE was dominated by diffusion. Under the optimized experimental conditions and square wave voltammetric parameters, the poly($[Cu(H_2O)_2P_2]I_2$)/GCE revealed very wide responses in the range of concentration of 500 nM–160 μM with a limit of detection of 3.91 nM and a Limit of quantification of 13.02 nM with the relative standard deviation below 1.75 %. The valuable applicability of the fabricated sensor for the determination of TMP in real samples, including cow's milk, blood serum, and human urine, was successfully investigated. The electroanalysis results from the spike recovery and interference study provided an excellent range of recovery with an error percent of below 3.0 % in the combination effect with the potential interferents. The sensor exhibited excellent reproducibility, sensitivity, long-term stability, high accuracy, and fast response. The developed bioanalytical sensor revealed the best application prospect for biomedicine and environmental monitoring activities.

1. Introduction

Trimethoprim (TMP), whose IUPAC name is 5-(3,4,5-trimcthoxybenzyl) pyrimidine-2,4 diamine is the family of sulfonamide class, which belongs to the chemotherapeutic agents called dihydrofolate reductase inhibitors [1]. This artificial antibiotic inhibits the synthesis of tetrahydrofolic acid and is used to treat urinary tract infections and prevention. TMP is also used to inhibit bacterial enzymes commonly in combination with sulfamethoxazole. This combination is known as co-trimoxazole [1].

TMP is also a broad-spectrum antibiotic that has antibacterial activity against most gram-positive bacteria and gram-negative bacteria. Additionally, TMP is prescribed for some infections like prophylaxis in HIV- affected patients at risk of pneumocystic jirovecii pneumonia, whipples diseases, and hematological malignancies. Although the use of TMP is widespread, it has many health

* Corresponding author. Department of Chemistry, College of Science, Bahir Dar University, Ethiopia.
E-mail address: melakumetto@gmail.com (M. Metto).

https://doi.org/10.1016/j.heliyon.2024.e38794
Received 6 August 2024; Received in revised form 24 September 2024; Accepted 30 September 2024
Available online 10 October 2024

problems: it sometimes contradicts during pregnancy, especially in the first trimester, and causes certain blood disorders [2]. It can also lower the levels of folic acid and the resulting development of bone marrow blood cells at renal tubules, which can result in dangerously low levels of thrombocytes.

A serious resistance mechanism had emerged despite a high degree of clinical success, necessitating a high dose regimen and novel pharmacokinetic combination. Furthermore, it is essential to create a straightforward, affordable, and user-friendly technique to ascertain the concentration of TMP from human bodily fluids and clinical samples due to its widespread usage and the risks it poses to humans and the environment. To date, there are a large number of analytical methods that have been established for the determination of trimethoprim from different samples. These include spectrophotometry [3], molecular imprinting chemiluminescence [4], polarography, adsorptive stripping voltammetry [5], and HPLC [6]. But most of the methods have their limitations, such as they lack sensitivity and selectivity, they are time-consuming, they require expensive equipment and complex sample pretreatment, they may require high cost, they also need skilled personnel, and they are simply energy-consuming. This type of complication can be solved by using electrochemical methods because they are widely used for their advantages of cheap equipment, ease of sample preparation, simple operation, rapid detection, and miniaturization [7]. Only a few electrochemical techniques for the analysis of TMP have been published to date, and they can demonstrate greater selectivity and sensitivity than the other widely used methods [8]. Electrochemical methods, including voltammetry, are fast, accurate, reproducible, and environmentally friendly. They are also often selective for the determination of electroactive antibiotics.

Surface activation of the sensor electrode by modification results in the formation of immobilized materials with a certain chemical and physical identity, which modifies the electrode's surface covering [9,10], improves compatibility and electrical conductivity and enhances mechanical properties and surface area [11]. The modification strategies of the given electrode have been done by employing electroactive matrices such as polymers, polymeric composites, nanomaterials, organometallic complexes, quantum dots, and some alloys [12–14]. Electrochemical sensors are unique in that they may be modified to improve their sensitivity and/or selectivity. They also stand out for their chemical and physical properties [15]. Among them, transitional metal-based materials such as complexes and conducting polymers are most commonly utilized for electrode modification either by potentiostatic electropolymerization [16], potentiodynamic electropolymerization [17], or simple surface coating [18] due to the unique features of metal complexes like high electrocatalytic activity, and wide application in the fabrication sensors [19,20].

Coordination chemistry researchers are interested in 1,10-phenanthroline (Phen), which serves as a chelating agent and is a bidentate ligand, is a crucial precursor in coordination chemistry and its derivatives because of their ability to interact with metal ions through the nitrogen atom they possess, which promotes the production of metal complexes [21].

Due to their unique properties, glassy carbon-based electrodes modified by transition metals complexed with organic ligands have recently attracted the attention of researchers, which include excellent electrocatalytic activity, high electrical conductivity, good capacitance, and good chemical stability [20,22]. On the other hand, transition metal complexes based on electrochemical sensors have become interesting in recent days. Potential applications in the electroanalysis of biological and pharmaceutical materials are considered for films produced electrochemically on the electrode surface [11].

Moreover, conducting polymers have attracted a lot of interest for analyte detection purposes, because of their strong adhesion to an electrode surface, chemical stability of the film, homogeneity, selectivity, and sensitivity in the electrochemical testimony of the electrodes modified by the polymerization process [23]. They have several advantages, such as low background current, chemical inertness, affordability, and a wide range of possible windows.

To the best of our knowledge, $[Cu(H_2O)_2P_2]I_2.H_2O$ has not been used as an electrode surface modifier, and poly($[Cu(H_2O)_2P_2]I_2$)/GCE has not been reported for electrochemical detection of TMP in clinical samples and cow's milk samples. The current study is focused on developing a technique that can precisely investigate trimethoprim in pharmaceutical fluid samples and local cow's milk samples using square wave voltammetry by achieving highly selective and sensitive strategies.

2. Experimental procedures and materials

2.1. Chemicals and apparatus used in this experiment

Metal salts of $CuCl_2.H_2O$ and KI (Analar BDH), 1,10-phenanthroline monohydrate (99.5 % Blulux laboratories (p) Ltd), Trimethoprim standard (99.7 %, Manus Aktteva Biopharma LLP laboratories (p) Ltd) from Ethiopian food and drug authority that is an analytical grade (99.0 %, Sigma Aldrich), analytical grade of potassium hexacyanoferrate a standard couple of $K_3[Fe(CN)_6]$ and $K_4[Fe(CN)_6]$ (98.0 %, BDH, England), K_2HPO_4 and KH_2PO_4 (98 %, Blulux laboratories (p) Ltd), highly pure KCl (99.5 %, from Blulux laboratories (p) Ltd), NaOH (Extra pure, Lab Tech Chemicals), and HCl (37 %, Fisher Scientific), were among the chemicals used. Exactly 0.5 M H_2SO4 solution was used for the stabilization of the bare and modified electrodes. The Phosphate buffer solutions (PBS) were prepared from 0.1 M KH_2PO_4, and 0.1 M K_2HPO_4 in deionized water, and the pH was adjusted by adding 1.0 M NaOH and 0.1 M HCl solutions.

CHN2200 elemental analyzer, Stuart SMP30 melting point apparatus, FTIR (PerkinElmer L1 600 400 Spectrum in the region 4000-400 cm^{-1}), Potentiostat with the series of CHI 760E (Austin, Texas, USA), AD8000, Romania pH meter, refrigerator (Lec refrigeration PLC, England), a centrifuge, an electronic balance (Nimbus, ADAM equipment, USA), and a water deionizer (Evoqua water technologies) were also among the tools and equipment utilized.

2.2. Synthesis of the complex

2.2.1. Synthesis of diaquabis(1,10-phenanthroline) copper(II) chloride ([$Cu(H_2O)_2P_2$]Cl_2)

With a few minor modifications, the published technique was used to prepare the intermediate complex [$Cu(H_2O)_2P_2$]Cl_2 [24]. A solution of 1,10-phenanthroline monohydrate (0.79 g, 4 mmol) in 40 mL of ethanol and water mixture in a 1:1 ratio was added from a dropping funnel to a solution of $CuCl_2$•$2H_2O$ (0.34 g, 2 mmol) in 40 mL of distilled water in a 250 mL round bottom flask being stirred magnetically in a water bath at room temperature. The result was a homogenous greenish-blue solution. The solvent was removed in a vacuum. A greenish-blue powder was collected and was washed using acetone three times. Then, the product was dried in the open air (yield: 0.89 g, 84 %).

2.2.2. Synthesis of [$Cu(H_2O)_2P_2$]l_2.$2H_2O$

The preparation of the target complex [$Cu(H_2O)_2P_2$]l_2.$2H_2O$ involved a straightforward metathesis reaction. 0.3 g of [$Cu(H_2O)_2P_2$]Cl_2 dissolved in 30 mL deionized water in a beaker was gradually added into a solution of potassium iodide (0.19 g) in 30 mL deionized water being stirred in a 100 mL round-bottomed reaction flask covered with aluminum foil to prevent iodide oxidation. As a result, brown precipitate development was seen right away. After 30 min of stirring, the mixture was left to stand for 1 h. The water was decanted, and the brown powder was gathered, washed three times with 20 mL distilled water each, placed in an open brown glass, and dried for 1 h at 60 °C in an oven (yield: 0.40 g, 94 %).

2.3. Procedures for analysis

2.3.1. Preparation of stock and working standard trimethoprim solutions

72.58 mg of monohydrated TMP powder was dissolved in deionized water to prepare the stock standard solution of 5 mM TMP in a 50 mL volumetric flask. Through serial dilution, the working solution of 1 mM TMP in 0.1 M phosphate buffer solution (PBS) with an appropriate pH was prepared from the stock solution. Every solvent used is of reagent-grade quality, and it is used exactly as it is supplied.

2.3.2. Electrochemical measurements

An electrochemical cell composed of a bare glassy GCE (PEEK Glassy Carbon Electrode, 3 mm diameter) or poly($Cu(H_2O)_2P_2$]I_2)/GCE as a working electrode, Ag/AgCl (3.0 M KCl) as a reference electrode and platinum coil as an auxiliary electrode was employed for all electrochemical measurements of the target solution. An electrochemical impedance spectroscopy (EIS) and cyclic voltammetry (CV) were used for the characterization of electrochemical behavior and the surface catalysis of the fabricated electrode using $[Fe(CN)_6]^{3/4-}$ as a probe, and again, the CV was used for the electrochemical qualitative investigation of TMP.

2.3.3. The fabrication of the Poly([$Cu(H_2O)_2P_2$]I_2)/GCE

Alumina slurries on a polishing cloth was used to polish the bare glassy carbon electrode to a mirror-like sheen, and it was then repeatedly washed with distilled water. After polishing, the electrode was left to dry at room temperature in the open. The potentiodynamic electropolymerization of the prepared [$Cu(H_2O)_2P_2$]I_2 complex was then done on the electroactive surface of the polished glassy carbon electrode by scanning in the range of potential between −1.1 V and 1.7 V at a scan rate of 100 mVs^{-1} for different cycles in the background solution of 1.0 mM of [$Cu(H_2O)_2P_2$]I_2.

After that, the newly prepared (poly($Cu(H_2O)_2P_2$]I_2)/GCE was rinsed with distilled water to remove any unreacted initial components from the electrode's activated surface. It was then stabilized in a freshly made monomer-free 0.5 M H_2SO_4 solution by scanning the electrode's potential over a wide potential range until a steady cyclic voltammogram was obtained and the electrode was assigned as poly($Cu(H_2O)_2P_2$]I_2 adsorbed glassy carbon electrode (poly($Cu(H_2O)_2P_2$]I2)/GCE). The developed sensors were utilized for electrochemical investigation after being cleaned with deionized water.

2.4. Optimization of experimental conditions

Experimental conditions, including the effect of film thickness, the effect of scan rate, and pH, were optimized. The contribution of film thickness to the electroactivity of the activated electrode was optimized by studying electrodepositing the monomer on the surface of the fabricated electrode with a varied number of cycles (16, 18, 20, 22, and 25 cycles). The investigation of scan rate on peak current and peak potential of a given species is the key function for studying the electrochemical parameters of such compounds of interest like reversibility of the redox behavior, rate-determining steps, type, or number of protons involved in the reaction and the ratio of electrons to protons [25–28]. The impact of scan rate on TMP oxidation behavior was investigated across scan rates of 10–300 mv/s. To investigate the effect of pH on the oxidative peak current and potential 1.0 mM TMP at various pHs (4.0, 4.50, 5.0, 5.50, 6.0, 6.50, 7.0, 7.50, and 8.0) were studied using poly([$Cu(H_2O)_2P_2$]I_2)/GCE in PBS by cyclic voltammetry.

2.5. Sample collection and real sample preparation

The urine and blood serum samples that were left over were taken by ice bag from the laboratory of the Tibebe Ghion Hospital in Bahir Dar, Ethiopia. The samples were kept for a full day in the refrigerator. A sample of fresh, raw cow's milk was also bought at the local Ethiopian market in Bahir Dar City.

2.5.1. Blood serum sample

A 15 mL fraction of the serum sample was centrifuged for 15 min at 4000 rpm in order to exclude any undesired precipitated components. The working solutions of the serum samples were prepared by transferring 5 mL of the supernatant to a 25 mL flask and diluting it with PBS at a pH of 6.50 (1:5) in order to determine the amount of TMP in the sample that was collected. Furthermore, by preparing various concentrations of standard TMP solutions and spiking them into the serum samples, the spike recovery was examined.

2.5.2. Human urine sample

In order to eliminate any solid components, a part of the urine sample that was obtained was centrifuged for 10 min at a speed of 4000 rpm. To determine whether the developed sensor could be used in real life, 5 mL of the supernatant fraction was transferred into a 25 mL flask and filled to the mark with PBS at pH 6.50. To verify the technique and investigate spike recovery, various concentrations of the standard TMP solutions were made and spiked to the sample.

2.5.3. Cow's milk samples

With a few minor modifications, the methods previously published were used to prepare the milk samples for actual sample analysis and determination [29]. To put it briefly, 5.0 mL of acetonitrile was added to a 50.0 mL milk sample while it was continuously stirred for 15 min. The mixture was then filtered through Whatman filter paper to deproteinize and coagulate the raw milk [23]. After being pasteurized, a 10 mL milk sample was sonicated for 10 min to ensure equal mixing. The sample was well mixed, and after 20 min of sonication, the aggregate was centrifuged for 10 min at 4000 rpm to eliminate any undesired suspended material. The supernatant was evaporated. The working solution was prepared by mixing 5 mL with PBS of pH 6.50 after centrifuging. Lastly, an electrochemical analysis was carried out and the sample was spiked with various doses of TMP standard solution for spike recovery investigation.

3. Results and discussion

3.1. Synthesis of the $[Cu(H_2O)_2P_2)]I_2{\cdot}2H_2O$

The leisurely formation of $[Cu(H_2O)_2P_2]Cl_2$ (Scheme S1 & eq. (1)) is attributed to the classic chelating bidentate ligand properties of 1,10-phenanthroline due to the cooperative contributions of its ideally placed nitrogen atoms, its rigid planar structure and π-acidic properties [30]. Moreover, the easy formation of $[Cu(H_2O)_2P_2]I_2.2H_2O$ was attributed to the easy anion exchange due to the comparable softness of $[Cu(H_2O)_2P_2]^{2+}$ and I^- [31].

The complex formation can be represented by equations (1) and (2) and Scheme S1:

$$CuCl_2{\cdot}2H_2O + 2P.H_2O \longrightarrow [Cu(H_2O)_2(P)_2]Cl_2 \quad \text{eq.1}$$

$$[Cu(H_2O)_2(P)_2]Cl_2 + 2KI \longrightarrow [Cu(H_2O)_2(P)_2]I_2.2H_2O \quad \text{eq.2}$$

Where P = 1,10-phenanthroline.

$[Cu(H_2O)_2P_2]Cl_2$ is a bluish-green solid. It is soluble in acetonitrile and water, slightly soluble in methanol, but insoluble in ethanol and acetone. $[Cu(H_2O)_2P_2)]I_2{\cdot}2H_2O$ is a brown non-hygroscopic powder that is slightly soluble in water, soluble in acetonitrile, ethanol, and methanol.

3.1.1. Molar conductance of the complexes

The electrolytic conductivity test recorded for 1 mM solutions of the complexes in acetonitrile is listed in Table S1. The result confirmed that both complexes are 1: 2 electrolytes [32]. The lower conductance of $[Cu(H_2O)_2P_2)]I_2{\cdot}2H_2O$ compared to $[Cu(H_2O)_2P_2]Cl_2$ is due to the increase in the mass of the counter anion, and its speed of mobility decreases. This is a result of the decrease in the

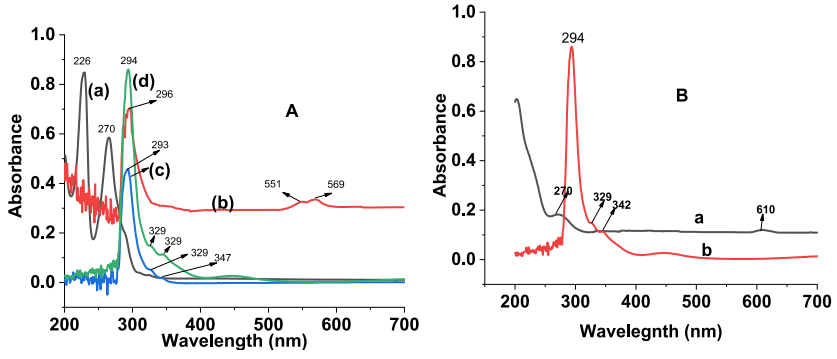

Fig. 1. A) Electronic spectra of a) 1,10-Phenanthrolinemonohydrate, b) $CuCl_2.2H_2O$, c) $[Cu(H_2O)_2P_2]Cl_2$, d) $[Cu(H_2O)_2P_2)]I_2{\cdot}2H_2O$ and B) the spectrum for complex monomer (a) and electropolymerized complex (complex polymer) (b).

kinetic energy supplied by the electric field from the measuring instrument [33]. The very good agreement between the data collected and the calculated CHN elemental analyses and Cu(II) and halide estimations results confirmed the reality of the assigned structures (Scheme S1).

3.2. Characterization of the complex

3.2.1. UV–Vis characterization

The electronic spectrum of the ligand complexes and the polymers are presented in Fig. 1. The electronic spectrum of the ligand shows two band maxima at 226 nm and 270 nm corresponding to π–π* and n-π* transition, respectively as shown in Fig. 1A (curve a). Since it is coordinated via the lone pair on the nitrogen, the band corresponding to the n-π* transition has disappeared (Fig. 1A, curves a and b). During coordination, there is electron flow from the filled t_{2g} orbitals of the metal ion to the empty π* of the ligand. This stops the π-π* transition. Consequently, the band at 226 nm in the spectrum of the ligand has disappeared (Fig. 1A, curves c and d). The band at 296 nm in the spectrum of the salt assigned to ligand to charge transfer is retained and slightly shifted to 293 nm in the complexes. However, the bands at 521 nm and 569 nm corresponding to $^2B_{1g} \rightarrow {}^2A_{1g}$ and $^2B_{1g} \rightarrow {}^2B_{2g}$, respectively disappeared in the complexes (Fig. 1A, curves b, c, and d) indicating the increase in the $^2B_{1g}$ - $^2A_{1g}$ and $^2B_{1g}$ - $^2B_{2g}$ gap following stronger bond formation due to the week basicity and strong acidic nature of 1,10-phenanthroline [34].

Additionally, as shown in Fig. 1B, the UV–Vis spectrum compared to the monomer spectrum verified the formation of the potentiodynamically electropolymerized polymer material on the electroactive surface of the electrode. On the polymer materials, there was a blue shift of the peak at 294 nm on the monomer complex, which was observed at 270 nm. The metal d-d orbital transition is responsible for the new band that emerged in the polymer's spectra at 610 nm. This could be due to the change of the coordinated ligand behavior in terms of field strength following the polymerization where the metal d orbital splitting is decreased eventually and absorbs at 610 nm.

3.2.2. FT-IR spectra

The selected IR spectral band of the ligand, the complexes, and the polymers are given in Fig. 2. The broad band at 3397 cm^{-1} in $[Cu(H_2O)_2P_2]Cl_2$ indicates the presence of coordinated water molecules concerning the metal ion (Fig. 2A, curve b). The bands at 3495 cm^{-1} and 3348 cm^{-1} in the spectrum of $[Cu(H_2O)_2P_2)]I_2{\cdot}2H_2O$ indicated the presence of water of crystallization and coordinated water molecules, respectively (Fig. 2A, curve c, Table S2) [35]. The band at 1622 cm^{-1} and 1588 cm^{-1} corresponding to υC=C in the spectrum of 1,10-phenanthroline is found shifted to 1631 cm^{-1}, 1583 cm^{-1} in $[Cu(H_2O)_2P_2]Cl_2$ and to 1625 cm^{-1}, 1584 cm^{-1} in $[Cu(H_2O)_2P_2)]I_2{\cdot}2H_2O$ indicating the change in the bond characteristic after the coordination. Furthermore, the change in the position and relative intensity of the bands at 1421 cm^{-1} in the spectrum of the ligand corresponding to δ_C=C (Fig. 2A, curve a and Table S2) to 1431 cm^{-1} and 1426 cm^{-1} in the complexes indicated the reduction of the freedom of bending following the coordination. Moreover, the new bands appeared at 426 cm^{-1} and 470 cm^{-1}, corresponding to Cu-N and Cu-O, confirming the coordination of the ligands to the metal center (Table S2).

On the other hand, the comparison between monomer complex and polymer has been investigated. Fig. 2B presents the IR spectrum of monomer and polymer formed by the potentiodynamic electropolymerization process. The distinct peaks observed in the spectra of the monomer complex either disappeared entirely or became substantially weaker in the polymer. The phenomena can be explained by a significant decrease in bond order after polymerization and dipole moments canceling out with the π electrons dispersed throughout the polymer.

Additionally, a prominent and characteristic band may be observed at 2265 cm^{-1} in the polymer spectrum. This band results from the conjugation of the π-bonds between C and N during polymerization. Because of this, the bond's Lewis basicity increased, which also increased the bond's strength (polymer peak).

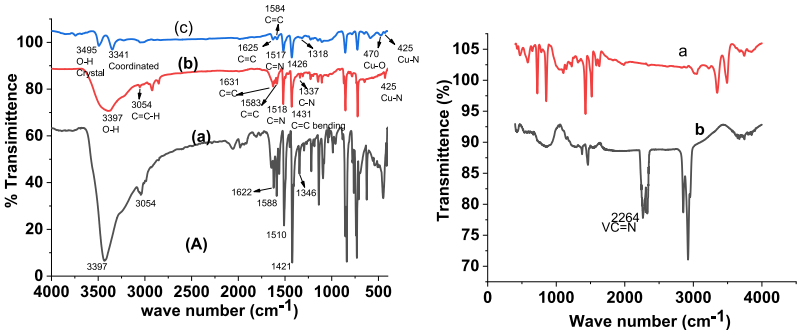

Fig. 2. A) FT IR spectra of a) 1,10-phenanthrolinemonhydrate, b) $[Cu(H_2O)_2P_2]Cl_2$, c) $[Cu(H_2O)2P2]I_2.2H_2O$, and B) FT-IR spectra of the monomer and electropolymerized complex.

3.3. Fabrication of Poly([Cu(H2O)2P2]I2/GCE

One of the most important parameters to consider for the polymerization of complicated monomers on the surface of the developed electrode was the potential scan range, which was followed by the film thickness. On the electrode surface, no film was deposited at potential windows that were narrower than −1.1 to +1.7 V. As a result, between −1.1 and + 1.7 V was the optimum potential window for the cyclic voltammetric electropolymerization of the complex at GCE.

Potentiodynamic electropolymerization of the poly($[Cu(H_2O)_2P_2]I_2$ polymer complex film occurred on the active surface of the glassy carbon electrode. This was accomplished by scanning the potential of the electrode for 15 cycles at a scan rate of 100 mV s-1 in a phosphate buffer solution (pH 7.0 PBS) containing 1.0 mM of $[Cu(H_2O)_2P_2]I_2$ complex.

During the electropolymerization of the complex monomer on the electroactive surface of the sensor, the presence of a visible oxidative peak at about (a) −0.02 V, (b) at about 0.40, (c) at about 0.7, (d) at about 1.1, and a broad reductive peak (a') centered at about −0.23 V and its oxidative peak current increased with scan number (Fig. S1). This confirms the electrodeposition of a redox-active polymer film on the surface of the GCE. The broad reductive peak (d) could be anticipated for molecular oxygen reduction. As can be seen from Fig. S1, the voltammograms of bare GCE (curve a of Inset A) and poly($[Cu(H_2O)_2P_2]I_2$)/GCE (curve b of inset A) in a monomer-free 0.5 M H_2SO_4 solution, a couple of two distinct redox peaks (a-a') at about −0.02 and −0.23 V only at the poly([Cu $(H_2O)_2P_2]I_2$)/GCE indicated deposition of a redox-active polymer film at the GCE surface for first and last cycles (curve a and b respectively for inset B of Fig. S3). Unlike the polymer-activated sensors electrode, the only cathodic peak (of curve A) that appeared at the bare GCE at a potential around 0.602 V which might be for molecular oxygen reduction, as shown in Fig. S1 inset (A).

3.4. Film thickness optimization

The influence of film thickness on the electrochemical feature of TMP in poly($[Cu(H_2O)_2P_2]I_2$)/GCE at PBS pH 7 in various cycles of deposition at a scan rate of 100 mVs^{-1} is shown in Fig. S2. It is evident from Fig. S2 that as the polymerization cycle increased, so did the anodic current response. This could result from taking into consideration the potential rise in effective surface area.

Initially, from 16 to 20 deposition cycles, the anodic peak current signal increased directly with increasing film cycles, as depicted in Fig. S3. This is because of the successive increase in the effective surface area of an electrode as the film thickness increases. Beyond 20 cycles, the oxidation peak signal response becomes reduced and almost equal to that of lower polymerization cycles. This could be because the electrode's effective active area is being reduced as a result of the modifier saturating its surface.

Furthermore, the emergence of an optimal sensing film at the GCE surface is indicated by the clean morphologies of the sharp oxidation peaks, which were recorded at a lower oxidative potential by 20 cycles. Consequently, the ideal film thickness for creating poly($[Cu(H_2O)_2P_2]I_2$)/GCE from its initial monomer material for the electrochemical analysis of TMP in particular samples from therapeutic formulations and bodily fluids was found to be 20 cyclic electropolymerization potential scan.

3.5. Characterization of the fabricated Poly([Cu(H2O)2P2]I2)/GCE

The electrochemical capability of the developed sensor electrode was investigated by cyclic voltammetry technique and electrochemical impedance spectroscopy (EIS). This study gave information about surface area improvement and charge transfer capacitance of the fabricated sensor electrode because of the adsorbed modifier on the surface.

3.5.1. Cyclic voltammetric study

The electrochemical activity of the polymer-modified working electrode was characterized by a cyclic voltammetric technique using poly($[Cu(H_2O)_2P_2]I_2$) modifier in $[Fe(CN)_6]^{3-/4-}$ as a redox probe. Results are shown in Fig. S4. A pair of reduction and oxidation peaks appearing on both bare (curve a) and poly($[Cu(H_2O)_2P_2]I_2$)/GCE (curve b) is attributed to a one-electron electrochemical process of $[Fe(CN)_6]^{3-/4-}$. The peak-to-peak potential separation (ΔEp) obtained indicates that the modified electrode exhibited enhanced electrocatalytic performance. In the case of the unmodified GCE, the peak-to-peak potential separation was 550 mV, whereas in the case of the poly($[Cu(H_2O)_2P_2]I_2$)/GCE, it was 106 mV. It confirms an improved charge transfer capacity of the polymer film [20, 36,37]. The higher electrode effective surface area may be the cause of the peak current enhancement at the modified electrode.

In addition, the ratio of oxidative to reductive peak current was also improved; I_{pa}/I_{pc} was 0.9 at bare GCE and 1 for that of poly([Cu $(H_2O)_2P_2]I_2$)/GCE modified GCE, indicating the reversibility of the system.

Fig. S4 shows that the functionalization of the electrode improves the results observed for $[Fe(CN)6]^{3-/4-}$. The peak potential difference between the bare GCE (curve a) and the poly($[Cu(H_2O)_2P_2]I_2$)/GCE (curve b) illustrates this. Additionally, the peak current improvement at the fabricated electrode, which is approximately 95 % of the current at the unmodified electrode, indicates the successful electrochemical polymerization of the monomer modifier onto the electroactive surface of the glassy carbon electrode.

Investigative research was done to verify that the GCE's electroactive region was enhanced upon modification by deposition. The result presented in Fig. S4 demonstrates how the cyclic voltammetric response of the bare and poly($[Cu(H_2O)_2P_2]I_2$) modified glassy carbon electrodes for $[Fe(CN)_6]^{3-/4-}$ varies with scan rate. This information was applied to compute the effective electroactive region of the electrodes by employing the Randles Sevcik equation (eqs. (3) and (4)) [38].

$$I_p = 0.4463nFAC\left(\frac{nFvD}{RT}\right)^{\frac{1}{2}} = 0.4463n^{\frac{3}{2}}FAC\left(\frac{FvD}{RT}\right)^{\frac{1}{2}} \quad \text{eq.3}$$

Since the experiment was conducted at room temperature (T = 298 k), the equation is simplified to:

$$I_p = 2.69\ x\ 10^5 AD^{1/2}n^{3/2}Cv^{1/2} \quad \text{eq.4}$$

Where $\mathbf{I_p}$ = Peak current (amperes), **n** = Number of electrons transferred in a redox cycle, **A** = The electrode surface area in working (cm^2), **C** = Molar concentration of redox-active species (mol/cm^3), **D** = The diffusion coefficient (cm^2/s), **v** = Scan rate in V/s and the constant has the unit of C mol^{-1} $V^{-1/2}$.

Taking n = 1 for $[Fe(CN)_6]^{3-/4-}$ because one electron is being transferred during the redox process and the diffusion coefficient of D = 7.6×10^{-6} cm^2/s for $[Fe(CN)_6]^{3-/4-}$ and $C_0 = 10^{-5}$ mol/cm^3, the electroactive surface area was calculated from the slope of the linear fit as shown in Fig. S5 (inset for A and B) of current versus square root of scan rate was 0.12 cm^2 for bare GCE, and 0.27 cm^2 for poly($[Cu(H_2O)_2P_2]I_2$)/GCE confirming that functionalization of the electrode increased the electroactive part of the electrode by about 225 %. The increased electrode surface area is the likely cause of the higher current measured for $[Fe(CN)_6]^{3-/4-}$ on the changed surface.

3.5.2. *Electrochemical impedance spectroscopic (EIS) characterization*

With the use of EIS, the electrodes' charge transfer kinetics were characterized comparatively [39]. EIS was applied to investigate an electrode's interface electrochemical properties. The Nyquist plots for unmodified GCE (a) and poly($[Cu(H_2O)_2P_2]I_2$)/GCE (b) in solution pH 7.0 PBS containing 10.0 mM $[Fe(CN)_6]^{3-/4-}$ can be observed in Fig. S6. As presented in Fig. S6, it is evident that both the untreated GCE and poly($[Cu(H_2O)_2P_2]I_2$)/GCE exhibited semi-circles of varying diameters at high-frequency regions and a line at approximately 45° at low-frequency regions. This is explained by the probe diffusing toward the electrode-solution contact from the bulk solution. Compared to the bare electrode (curve a), the poly($[Cu(H_2O)_2P_2]I_2$)/GCE (curve b) displayed a semi-circle with a significantly smaller diameter, indicating that the electrode surface was modified with an electroactive polymer film. The conductivity of the electrode surface is effectively increased by this film coating. At poly($[Cu(H_2O)_2P_2]I_2$)/GCE, the R_{ct} value decreased implying the deposition of highly conductive nanoparticles with a high surface area that acted as electron transfer channels.

Remarkably, when compared to the untreated electrode, poly($[Cu(H_2O)_2P_2]I_2$)/GCE showed the least amount of obstruction to electron transfer and the highest double-layer capacitance (Table S3). As a result, the EIS results closely support the electrode's surface activation as a result of alteration and line up with the findings of the CV investigation.

3.6. *The electrochemical activity of TMP on the fabricated electrode surface*

The electrochemical response of trimethoprim on Cyclic voltammetric investigation at poly($[Cu(H_2O)_2P_2]I_2$)/GCE was performed

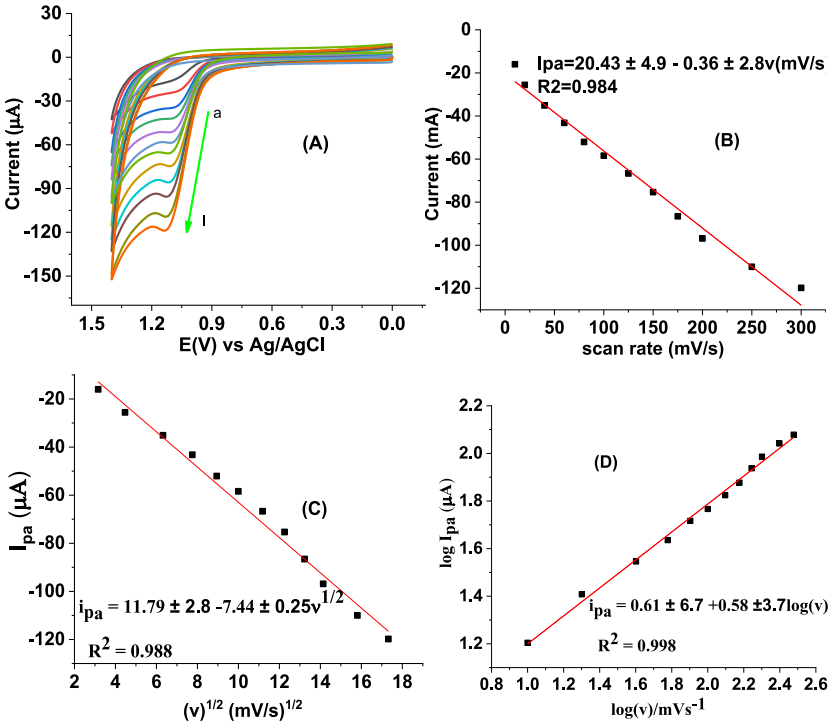

Fig. 3. (A) CVs of poly($[Cu(H_2O)_2P_2]I_2$)/GCE in PBS pH 7 PBS containing 1.0 mM TMP at various scan rates (a to l: 10, 20, 40, 60, 80, 100, 125, 150, 175, 200, 250, and 300 mV/s, respectively), (B) plot of Ip *vs.* scan rate, (C) plot of Ip *vs.* $(v)^{1/2}$, and (D) plot of log Ip *vs.* log(v).

by analysis of 1 mM TMP and compared with that of bare GCE (Fig. S7). As can be depicted in Fig. S7, the existence of a single well-resolved oxidation peak at around 850 mv potential and no peak response in the backward scan direction both at bare and poly([Cu(H_2O)$_2$$P_2$]$I_2$)/GCE for TMP (curves b and d, respectively). This is an indication of the irreversible oxidation of TMP at poly([Cu(H_2O)$_2$$P_2$]$I_2$)/GCE. The observed anodic peak at the poly([Cu(H_2O)$_2$$P_2$]$I_2$)/GCE (curve b of inset) with improved peak current around 3.2 folds of (over 45 μA) relative to the weak anodic peak at the unmodified GCE (curve a of inset) might be attributed to the high surface roughness and improvement of electrode effective region area of the polymer-modified electrode due to the deposition of the complex.

On the other hand, a shift in the peak potential was noted upon modification. The oxidative peak of TMP on bare GCE has appeared at Ep 1096 mV and poly([Cu(H_2O)$_2$$P_2$]$I_2$)/GCE at Ep 1069 mV). This shows that modification of the target electrode with polymer shifted the peak of formation at about 27 mV to the earlier side. The peak potential shift at poly([Cu(H_2O)$_2$$P_2$]$I_2$)/GCE is supposed to be the improvement of the charge transfer catalysis of the electrode [19,22,40,41]. The enhancement of trimethoprim's oxidative peak current and the lowering of its peak-to-peak potential at poly([Cu(H_2O)$_2$$P_2$]$I_2$)/GCE demonstrate the complex modifier's electro-catalytic ability to oxidize TMP.

3.7. Effect of scan rate

Fig. 3A represents cyclic voltammograms of TMP in pH 7.0 PBS at a range of scan rates. It can be observed that, as the scan rate increases, the shift of peak potential in the positive direction was observed. The shift of potential with scan is the confirmation of the irreversibility of TMP oxidation at poly([Cu(H_2O)$_2$$P_2$]$I_2$)/GCE. The linear relationship between peak current and scan rate (Fig. 3B) has a lower regression coefficient (Fig. 3C, $R^2 = 0.984$) than the relationship between peak current and the square root of scan rate ($R^2 = 0.988$). This indicates that the oxidation of TMP at poly([Cu(H_2O)$_2$$P_2$]$I_2$)/GCE is primarily diffusion-controlled [27,42]. Also, in the plot of log(Ip) versus log(v) (Fig. 3D), it can be indicated that the slope is 0.58, which indicates that the oxidation TMP is supposed to be a diffusion and adsorption-controlled process because it is between 0.5 and 1 for both processes. However, the result of 0.58 is highly close to the ideal value of 0.50 for a completely diffusion-controlled reaction [22], and other investigations confirm the diffusion process. This further confirms that the oxidation of TMP at the poly([Cu(H_2O)$_2$$P_2$]$I_2$)/GCE is highly controlled by diffusion than charge transfer [22,43,44].

To investigate the kinetic parameters, including the number of electrons participated and the electron transfer coefficient for the oxidation of TMP at poly([Cu(H_2O)$_2$$P_2$]$I_2$)/GCE, the Tafel equation (eq. (5)) was used. The Tafel equation clearly provides information about the electrons transferred and the coefficient of electron transfers during irreversible redox processes in cyclic voltammetric data. During the electroanalytical oxidation of TMP at the poly([Cu(H_2O)$_2$$P_2$]$I_2$)/GCE, the number of electrons that participated was determined from the cyclic voltammetric response by taking cyclic voltammetric response on 100 mv/s by determining the αn values from the irreversible process. The αn value was calculated by subtracting the half-wave potential ($E_{p1/2}$) from the peak potential (Ep) by using equation (eq. (5)) [45,46]:

$$E_p - E_{\frac{p1}{2}} = \frac{48}{\alpha n} \quad \text{eq.5}$$

Where α is the charge transfer coefficient, n is the number of electrons involved. At a scan rate of 100 mv/s, Ep and $E_{p1/2}$ for the cyclic voltammogram of TMP (Fig. 3A from scan rate) are found to be 1095 mv and 995 mV, respectively. The value of αn was computed to be 0.48. As described in the literature elsewhere [47], for totally irreversible electrochemical processes, the α value is considered to be 0.5. Taking this into consideration, for totally irreversible processes, the number of electrons (n) transferred in the electrochemical oxidation of TMP at the surface of poly([Cu(H_2O)$_2$$P_2$]$I_2$)/GCE was estimated to be 0.96 (~1.0).

The relationship between peak potential and lnv for irreversible electrochemical processes can be computed by obeying the following equation (eq. (4)) [47].

$$E_p = E^O + \frac{RT}{(1-\alpha)nF}\left\{0.780 + \ln\left(\frac{D_R^{\frac{1}{2}}}{k^o}\right) + ln\left[\frac{(1-\alpha)nFv}{RT}\right]^{\frac{1}{2}}\right\} \quad \text{eq.6}$$

Where E_p is the peak potential, E^o is the formal potential, α is the electron transfer coefficient, k^o is the electrochemical rate constant, R is the universal gas constant, F is Faraday's constant, T is kelvin temperature, and the other parameters are with their usual meanings.

From the plot of E_{pa} versus ln v (Fig. S8A), taking the slope 0.024, meaning (slope $= \frac{RT}{2(1-\alpha)nF} = 0.024$ for the fitted line ($E_{pa}(v) = 0.98 + 0.024$ ln v) of the curve.

At room temperature, the value of n(1–α) can be determined using the above equation (eq. (4)) and was obtained to be 0.53. Taking the one electron for oxidation of TMP calculated using eq. (4), the electron transfer coefficient (α) was found to be 0.47, which is remarkably close to 0.5, confirming the irreversibility of the oxidation of TMP [48].

In addition, Tafel slope b can be determined by applying eq. (7) to obtain the information on the rate-determining step which is valuable for a totally irreversible diffusion-controlled process.

$$E_p = b/2 \log(v) \quad \text{eq.7}$$

As can be depicted from Fig. S8B, and equation (7), the slope of the plot of E_{pa} vs log(v) is b/2, where b indicates the Tafel slope. From the plot of E_{pa} vs log(v), the slope was found to be 0.055 (Fig. S8B), and therefore, the value of Tafel slope b is equal to 0.11. The

Tafel slope value strongly confirms the one-electron transfer process in the rate-limiting step assuming a transfer coefficient to be 0.54 [49,50].

3.8. The impact of pH on the peak responses

One significant element influencing trimethoprim's peak current and potential at poly([$Cu(H_2O)_2P_2$]I_2)/GCE is the pH value of the supporting electrolyte. This can provide valuable information regarding the involvement of protons in redox reactions of the electrochemical process, the possible ratios of electrons and the proportion, and the proposed mechanism of the interaction between the electrode surfaces and the interacting species. Hence, investigating the pH effect is an indispensable parameter. The shift of the peak potentials towards the negative potential directions as the pH of the electrolyte increases from 4.0 to 8.0, ss can be observed from the graphs, (Fig. 4A), this is evidence that the proton is involved in the electrochemical redox reaction of TMP at the poly([$Cu(H_2O)_2P_2$]I_2)/GCE surface. The oxidative peak potential vs pH plot shows that protons and electrons participate in a 1:1 ratio, as indicated by the slope of 0.048 V (curve a from Fig. 4B). Scheme S2 presents the proposed mechanism of electron and proton transfer in the oxidation reaction of TMP [51,52]. In contrast, the electrochemical oxidative peak current of TMP at the surface of poly([$Cu(H_2O)_2P_2$]I_2)/GCE was observed to increase with pH value from 5.0 to 6.5 after then decreasing at pH values beyond 6.5 (curve b of Fig. 4B). The increase of the oxidative peak signal of TMP at acidic regions might be a result of the interaction of the TMP with the electrode-modifying materials. (pKa ≈7.4) [53].

3.9. Quantitative investigation of TMP at Poly([$Cu(H_2O)_2P_2$]I_2)/GCE

Since square wave voltammetry (SWV) is the most effective electroanalytical technique for separating the faradaic current from the non-faradaic one and can be useful in detecting an exceptionally low detection limit and high sensitivity, it was used for the quantitative analysis of Trimethoprim in clinical and biological samples [54]. Fig. S9 presented the SWV responses of PBS at pH 6.50 with and without 1.0 mM TMP at bare and poly([$Cu(H_2O)_2P_2$]I_2)/GCE and their corresponding voltammogram of background corrected bare (curve of inset a) and poly([$Cu(H_2O)_2P_2$]I_2)/GCE (inset b of Fig. S9). As presented in Fig. S9, a well-shaped and highly intensive square wave voltammogram was observed, with a current performance that was about 7.7 times greater and a potential reduction of approximately 80 mV. This is the confirmation of the contribution of the polymer as the catalytic activator of the electroanalytical oxidation of TMP towards poly([$Cu(H_2O)_2P_2$]I_2)/GCE.

3.10. Optimization of the SWV parameters

For the real applicability of the developed sensor for TMP analysis, the square wave voltammetric parameters (step potential, pulse amplitude, and frequency) should be optimized to get the best responses. The behavior of peak intensities upon the step potential, square wave amplitudes, and frequency were optimized by making a conciliation between the increased Faradaic peak current and accompanied capacitive current [21].

3.10.1. Effect of step potential

The influences of stepping potential on the intensities and shapes of the electrochemical oxidation current of TMP on poly([$Cu(H_2O)_2P_2$]I_2)/GCE to invest the appropriate potential at which the SWV can be stepped. The anodic current signal response of 1.0 mM TMP at the poly([$Cu(H_2O)_2P_2$]I_2)/GCE revealed an increase with step potential in the range of potential from 2 to 10 mV (Fig. S10). As illustrated in the inset of Fig. S10, however, the anodic peak signal increase is followed by a loss in peak intensity range and linearity exhibited beyond 4 mV. Due to the increased Faradaic current and potential shift, a step potential of 4 mV has been chosen to be the optimum step potential for additional square wave voltammetric measurement.

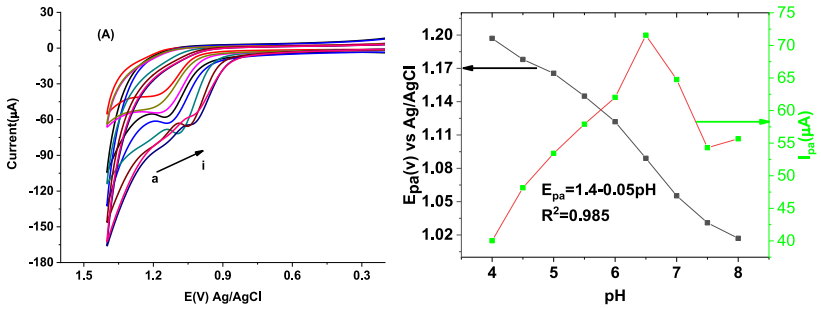

Fig. 4. (A) CVs of poly([$Cu(H_2O)_2P_2$]I_2)/GCE in PBS at the range of pHs (a–i: 4.0, 4.5, 5.0, 5.5, 6.0, 6.5, 7.0, 7.5, and 8.0, respectively containing 1.0 mM TPM, (B) plot of (a) peak current and (b) peak potential *vs.* pHs in the entire pH range.

3.10.2. Study of square wave amplitude

The impact of square wave amplitude on the anodic peak current signal response of TPM at the poly([$Cu(H_2O)_2P_2$]I_2)/GCE was implemented in the range of wave amplitude from 15 to 40 mV (Fig. S11). As the square wave amplitude increases from 15 to 40 mV, the peak current also increases. The current symmetry was linear from 15 to 25 mV, and beyond 25 mV, As shown in Fig. S11 (inset), there was a slight increase in the peak current beyond 25 mV. A compromise was reached between the corresponding peak broadening and the peak current increment, and a square wave amplitude of 25 mV was chosen to be optimal.

3.10.3. Effect of frequency

Another key factor that determines the square wave voltammogram response of poly([$Cu(H_2O)_2P_2$]I_2)/GCE on oxidation of TMP is square wave frequency. The SWVs of 1.0 mM TPM at the fabricated electrode at various frequencies, i.e., 10–40 Hz, are presented in Fig. S12. The response of the electrode towards TPM varied with frequency, showing an increase in a similar trend as observed for the effect of amplitude. The rise in the frequency of the pulse was ascribed to the improvements in the current values in all studied extensions (inset of Fig. S12), but for values higher than 20 Hz, the symmetry of current intensities decreased. A frequency value of 20 Hz was chosen for further investigation reasons as for those for the square wave amplitude and step potential.

3.11. Calibration method and detection limit

A calibration curve for the investigation of TMP was performed by an investigation of the SWV response of the developed electrochemical sensor electrode for varied concentrations of standard TMP. Fig. 5 shows the SWV signals of the various concentrations of trimethoprim under optimum conditions, solutions, and SWV method parameters. The average anodic peak current response of TMP (for triplicate measurement) was linearly varied within the range of concentrations 0.5–160.0 μM. The developed sensor revealed a LOD of 3.91 nM and a LOQ of 13.02 nM, which were calculated as 3 s/m for n = 7 and 10 s/m, respectively. Inset of Fig. 5). The precision of the fabricated biosensor based on the novel mixed organic ligand with Cu(II) complex as electrode modifier was demonstrated through triplicate measurements, with an associated %RSD of 1.67 %.

3.12. Analytical application and validation of the sensor for determination of TMP in real sample

The analytical utilization of the developed poly([$Cu(H_2O)_2P_2$]I_2)/GCE-based electrochemical sensor for real-life application was studied by investigation of TMP from biological and clinical samples. The fabricated sensor was successfully utilized to investigate the TMP from urine, clinical blood serum, and cow's milk samples. In addition, further investigation was conducted on the reliability of the proposed Poly([$Cu(H_2O)_2P_2$]I_2)/GCE-based sensor to ensure its accuracy in detecting TMP in real samples, such as human blood serum, cow's milk, and urine. To achieve this, the study was done on the recovery of spiking standards, interference analyses, stability testing, and repeatability assessment of the fabricated sensor.

3.12.1. Blood serum sample

For real sample analysis, the fabricated electroanalytical sensing electrode was applied for the diagnosis of TMP in a human blood serum sample. Fig. 6A presents the peak signal response of the blood serum sample with and without containing variable concentrations of TMP. No distinctive peak is present in the sample, and the peaks appeared as a result of spiking specific TMP concentrations. The absence of detectable levels of TMP in the examined human blood serum samples is shown by the characteristic peak signal not

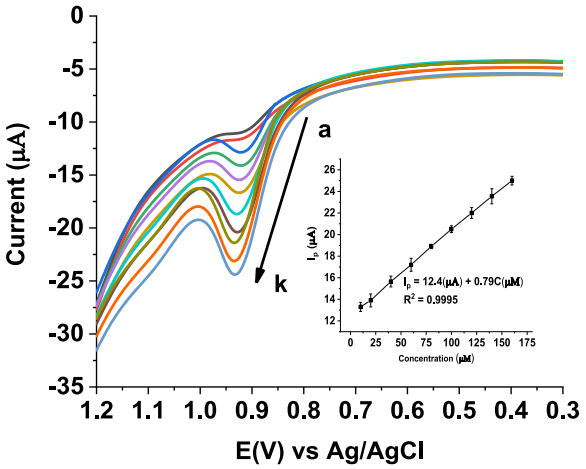

Fig. 5. Blank subtracted SWVs of poly([$Cu(H_2O)_2P_2$]I_2)/GCE in PBS of pH 6.50 for different concentrations of TMP (a–k: 0.5, 1.0, 5.0, 10.0, 20.0, 40.0, 60.0, 80.0, 100, 120, and 160 μM, respectively) at a step potential 4 mV, amplitude 25 mV, and frequency 20 Hz. Inset: plot of anodic peak response *vs.* concentration of TMP.

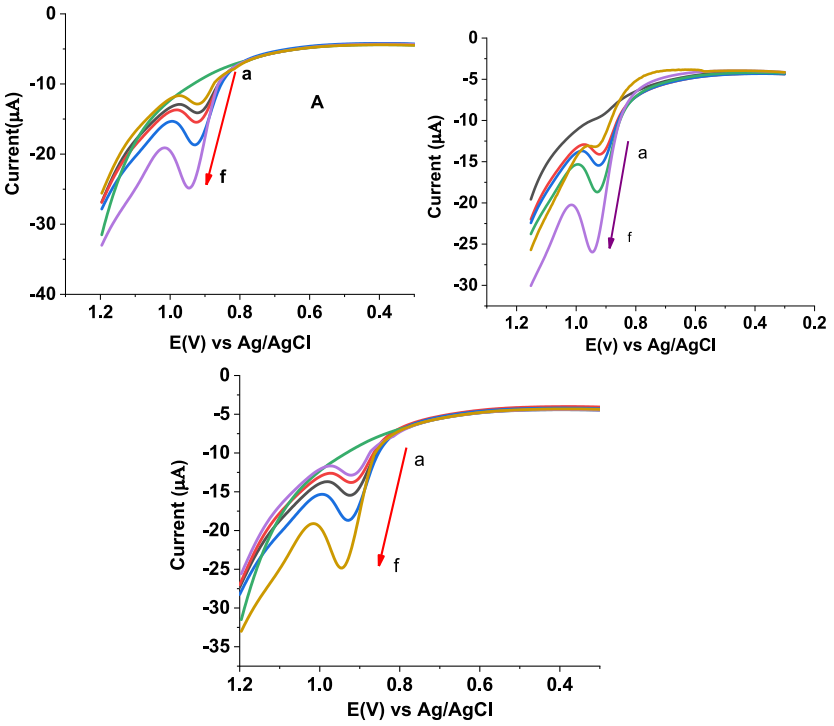

Fig. 6. Background Corrected Square Wave Voltammograms of poly([Cu(H$_2$O)$_2$P$_2$]I$_2$)/GCE in pH 6.50 PBS containing A) blood serum, B) urine, and C) cow's milk samples with a) unspiked samples b) a +10.0 μM standard TMP, c) a +20.0 μM standard TMP, d) 40 μM standard TMP, e) a +80.0 μM standard TMP, and f) a +160.0 μM standard TMP, at a stepping potential of 4 mV, amplitude of 25 mV, and frequency of 20 Hz.

appearing. The spike recovery investigation results represented in Table 1 indicate excellent recovery in the range between 99.70 and 102.05 %, confirming that the developed method for effective determination of TMP in biological fluids like human blood serum was accurate. The results designate that the recovery data, as shown in Table 1, confirms that the developed method is suitable for determining the presence of TMP in human blood serum samples.

3.12.2. Human urine sample

Additionally, an analysis of a human urine sample taken from the hospital by SWV was conducted to verify the true pertinence of the developed poly([Cu(H$_2$O)$_2$P$_2$]I$_2$)/GCE. SWV for a clinical human urine sample prepared in accordance with the method previously outlined in the experimental procedure is shown in Fig. 6B. It is possible to infer from Fig. 6B that the signal lacking a typical peak

Table 1
An overview of the recovery results for various TMP concentrations spiked in blood serum, urine, and cow's milk samples.

Sample	Added standard (μM)	Expected (μM)	Found (μM)[a]	% Recovery
Serum Sample	0	0	0	0
	10	10	9.97 ± 0.07	99.70 ± 1.45
	20	20	20.37 ± 0.29	101.85 ± 2.57
	40	40	40.75 ± 0.92	101.87 ± 2.63
	80	80	81.64 ± 1.16	102.05 ± 2.31
	160	160	160.76 ± 4.13	100.46 ± 3.45
Urine Samples	0	0	0	–
	10	10	10.25 ± 0.26	102.50 ± 1.32
	20	20	20.50 ± 0.26	102.50 ± 2.34
	40	40	40.37 ± 1.02	100.93 ± 1.35
	80	80	81.11 ± 2.50	101.38 ± 2.11
	160	160	165.80 ± 0.71	103.62 ± 3.12
Milk Samples	0	0	0	–
	10	9.75 ± 2.32	10	97.50 ± 2.33
	20	20.75 ± 3.43	20	103.75 ± 4.21
	40	41.14 ± 2.24	40	102.85 ± 2.44
	80	80.88 ± 1.76	80	101.10 ± 2.32
	160	160.87 ± 4.21	160	100.54 ± 2.42

[a] mean ± SD for triplicate measurements.

signal at the potential range of TMP oxidation suggests that the human urine sample under analysis did not contain active TMP, while the spiked samples did exhibit characteristic peaks.

The extended applicability of the now suggested sensor for real sample analysis was successfully studied by the spike recovery analysis, which involved adding 10, 20, 40, 80, and 160 μM standard solutions of TMP to the urine sample, in order to further confirm recovery. From Fig. 6B, the spiked standard TMP generated sharp peaks regardless of their concentrations with respective potential and current intensities. The spiked standard solutions provided an excellent recovery result within the range of recovery of 100.93–103.62 % as described in Table 1. The data from the spike recovery study thus validates the accuracy, precision, and suitability of the electrochemical sensor for TMP analysis in biological and pharmacological substances.

3.12.3. Cow's milk sample

Analysis of local cow's milk samples under optimal conditions for experiments and SWV parameters was done to explore the wider use of the proposed sensor for accurate and precise estimation of TMP. The SWV response of the cow's milk sample collected from Bahir Dar City was presented in Fig. 6C. It is evident from Fig. 6C that the voltammetric signal lacking a peak at the characteristic potential of TMP suggests that the milk sample under analysis does not contain active TMP, while the spiked samples did exhibit characteristic peaks.

Additionally, the recovery of the spike study of TMP in samples of cow's milk was examined to assess the validity and accuracy of the present approach. Table 1 illustrates the good spike recovery that was accomplished. The accuracy of the devised sensor for determining TMP in samples of cow's milk is also tested, confirming its validity as presented in Fig. 6C. The developed sensor's efficacy in diagnosing the target species is confirmed by the high recovery shown in the spike recovery result, which falls between 97.50 and 103.75 %.

3.13. Interference study

The selective investigation of TMP in the presence of possible interfering matrices was examined in the interference analysis of the complex polymer-modified electrochemical sensor. The selectively detecting ability of the current method for the TMP presence of guanine, sulfamethoxazole, and salbutamol was analyzed by adding various concentrations of each (0–60 μM) on the signal response of 30 μM TMP as presented in Fig. 7. The current sensor's signal response was excellent in detecting the targeted TMP, even in the presence of possible interferents such as salbutamol (Fig. 7A), guanine (Fig. 7B) and sulfamethoxazole (Fig. 5C) at concentrations up to two times higher and the resulting bar graph is presented as (Fig. 7D). The recovery rate was also exceptional, with an associated error

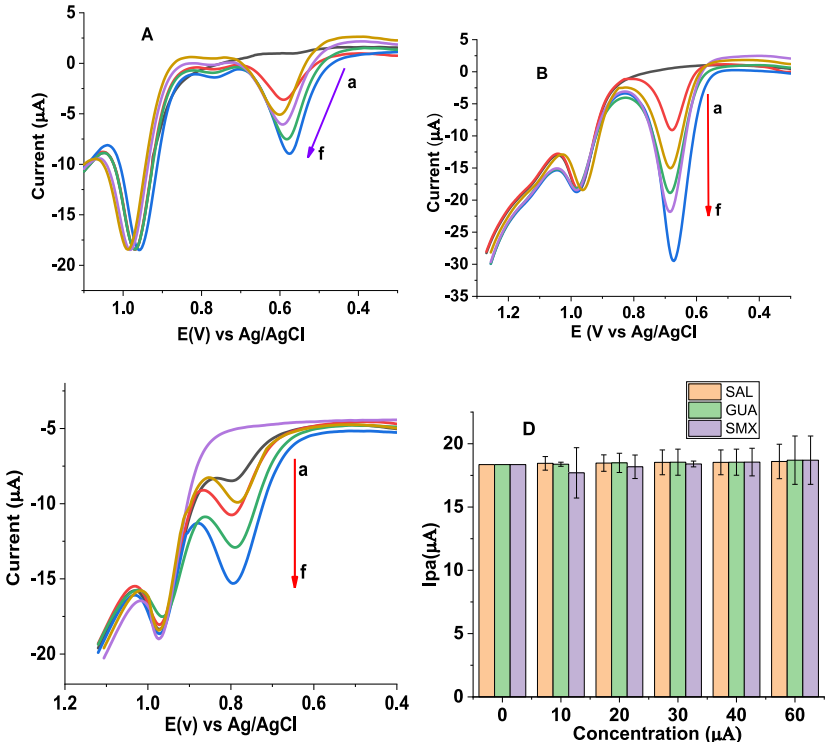

Fig. 7. Background subtracted SWVs of poly([Cu(H_2O)$_2$$P_2$]$I_2$)/GCE in pH 6.50 PBS containing 30 μM TMP standard solution containing A) salbutamol, B) Guanine, C) Sulfamethoxazole of various concentrations a – f; 0, 10, 20, 30, 40 and 60 μM respectively, at a stepping potential of 4 mV, square wave amplitude of 25 mV, and frequency of 20 Hz, and the resulting bar graph for each interferent.

of less than 2 %. The study revealed the accuracy and selectivity of the proposed poly([$Cu(H_2O)_2P_2$]I_2)/GCE-based electrochemical sensor to be highly effective for the qualification and quantification of the TMP from clinical human serum and urine samples.

The TMP's current signal response is summed up in Table 2 both in the absence of potential interferents and their presence.

Table 2 summarizes the current signal response of the TMP without interfering substances and in the presence of potential interferants. It was discovered that the proposed method's recovery value fell between recovery 98.66 and 102.70 %, with an error of less than 3 % for measurements made in triplicate. This suggests that the suggested sensor can be used to accurately determine TMP in real samples even when there are possible interfering species present.

In addition, as seen in Fig. S13, TMP displayed peak currents with an inaccuracy of less than ±5 % of that of the pure solution in the presence of interfering compounds and ions such as salbutamol, guanine, sulfamethoxazole, K^+, Na^+, Cl^- and NO_3^-. Thus, it can be concluded that the suggested sensor is selective and appropriate for TMP detection since these chemicals do not interfere with TMP detection.

3.14. Stability and reproducibility study

The long-term stability, reproducibility, and applicability of the current method were investigated. The %RSD of the developed biosensor for selective and reproducible measurements for the quintuplicate SWV readings of the sensor in pH 6.50 PBS containing 40.0 μM TMP recorded at an interval of 2 h in a day (Fig. S14) and for 16 successive days (Fig. S15) with SWVs at an interval of three days. The %RSD for both intraday and interday stability were 1.12 % and 1.78 %, respectively, and an error was found below 5 % for multiple measurements of the current of a fixed concentration of TMP. This result depicts that the developed polymer film-based electrode is highly stable for qualitative and quantitative determination of TMP as a result of the stability of the polymer film.

Tables S3 and S4 provide a summary of the stability results of the fabricated biosensor for long-term applicability in determining TMP from real samples. Based on the data, it can be strongly suggested that the developed sensor is highly stable, with excellent accuracy and recovery results of above 95 %. Overall, after 16-day storage, the intensity of the current reduced was 0.86 μA which is about 4.93 %, indicating the best shelf life of the polymeric material on the surface of the electrode.

Thus, the current sensor electrode confirms its validated applicability for the determination of TMP in real samples with a complex matrix, such as human blood serum, human urine, and cow's milk samples. It also has excellent spike recovery, stability, and interference recovery results in addition to a wide linear range, low LOD, and LOQ results.

3.15. Performance evaluation of the current method

The characteristic routine application of the proposed technique for quantification of trimethoprim was compared with those beforehand reported methods from the literature, as illustrated in Table 3. The Fig.s of merit of the new sensor in terms of limit of detection, linear dynamic range, nature of the substrate, and the type of modifier were highly efficient for the assessment of TMP from real samples.

4. Conclusion

The effective synthesis of a 1,10-phenanthroline-based new [$Cu(H_2O)_2P_2$]I_2 complex was confirmed by UV–Vis and FT-IR data characterization results. The sensor was fabricated by potentiodynamically electropolymerization deposition of [$Cu(H_2O)_2P_2$]I_2 film on the electroactive region of a GCE. The surface improvement of the electrode due to the deposition of Poly[$Cu(H_2O)_2P_2$]I_2 film was

Table 2
Summary of interference recovery studies of TMP in the presence of 100.0–60.0 μM of DIC and SAL.

Interferent	Interferent added (μM)	Detected Current (μA)[a]	Expected current(μA)	Recovery[a]	%Error[a]
SAL	0	18.35 ± 0.04			
	10	18.45 ± 0.14	18.35	100.54 ± 3.23	−0.54 ± 2.67
	20	18.47 ± 0.11	18.35	100.65 ± 2.10	−0.65 ± 2.76
	30	18.53 ± 0.27	18.35	100.98 ± 0.12	−0.98 ± 1.98
	40	18.53 ± 0.44	18.35	100.98 ± 2.82	−0.98 ± 2.84
	60	18.60 ± 0.15	18.35	101.36 ± 1.23	−1.36 ± 2.34
G	0	18.35 ± 0.33			
	10	18.38 ± 0.19	18.35	100.16 ± 2.01	−0.16 ± 2.10
	20	18.49 ± 0.47	18.35	100.76 ± 1.92	−0.76 ± 1.20
	30	18.54 ± 0.36	18.35	101.03 ± 2.81	−1.03 ± 4.12
	40	19.54 ± 0.13	18.35	101.03 ± 1.91	−1.03 ± 2.45
	60	18.70 ± 0.24	18.35	101.91 ± 0.32	−1.91 ± 3.35
SMX	0	18.35 ± 0.42			
	10	17.80 ± 0.14	18.35	97.00 ± 4.24	2.99 ± 2.35
	20	18.18 ± 0.35	18.35	99.07 ± 1.67	0.93 ± 2.71
	30	18.40 ± 0.27	18.35	100.23 ± 2.36	−0.23 ± 2.78
	40	18.55 ± 0.41	18.35	101.09 ± 3.45	−1.09 ± 3.12
	60	18.70 ± 0.39	18.35	101.91 ± 2.43	−1.91 ± 1.23

[a] mean ± SD for n = 3.

Table 3
Comparison of several types of electrodes reported for investigation of TMP with the current study.

Electrode	Technique	pH	LDR(μM)	LOD (μM)	Ref.
GR-ZnO/GCE	DPV	7.0	1–170	0.3	[7]
G-CPE	DPV	3.4	0.9–100	0.02	[55]
MIP@Fe3O4@MWNTs/rGO/MCPE	DPV	–	0.004–500	1.2	[56]
AuNPs-Printex(6L)- CTS: EPH/GCE	SWV	4.0	0.20–6.0	0.0124	[8]
CuPh – PC/GCE	SWV	7.0	0.4–6.0	0.67	[57]
poly($[Cu(H_2O)_2P_2]I_2$)/GCE	SWV	6.5	0.5–160	0.0039	This work

investigated and confirmed by CV and EIS techniques. The Poly($[Cu(H_2O)_2P_2]I_2$)/GCE demonstrated remarkable electrocatalytic activity on the oxidation of TMP in PBS due to the synergistic effect of elevated electrode effective surface area and electrical conductivity. The study of the scan rate confirmed the rate-determining oxidation of TMP, which was an utterly diffusion-controlled process. The quantitative electrochemical investigation of TMP in pharmaceutical urine and serum samples and cow's milk on poly($[Cu(H_2O)_2P_2]I_2$)/GCE was determined by square wave voltammetric methods. The outstanding stability, reproducibility, excellent spike recovery, and interference results, wide dynamic concentration range, and sufficiently low limit of detection validated the usability of the proposed technique for TMP assessment in pharmaceutical samples and cow's milk. The effectiveness of the developed sensor for TMP determination was confirmed by the recovery of the present technique on the analyzed samples, which was determined to be in the range between 97.50 and 103.75 % on their various spiked labels. The current approach demonstrated the best performance compared to previously published methods, making it a great option for determining TMP in samples with complex matrices, such as cow's milk, serum, and other pharmaceutical samples in the presence of potential interfering materials.

CRediT authorship contribution statement

Melaku Metto: Writing – original draft, Methodology, Investigation, Formal analysis, Data curation, Conceptualization. **Alemu Tesfaye:** Writing – review & editing, Supervision, Investigation, Conceptualization. **Minaleshewa Atlabachew:** Writing – review & editing, Supervision, Resources, Investigation, Data curation, Conceptualization. **Atakilt Abebe:** Writing – review & editing, Supervision, Methodology, Investigation, Formal analysis, Data curation, Conceptualization.

Data availability statement

The dataset used and/or analyzed in the current study is available from the corresponding author on request.

Ethical approval and consent

There is no applicable ethical consideration for this work.

Agreement for publication

The authors have agreed to the publication of this work upon its acceptance.

Declaration of competing interest

The authors declare the following financial interests/personal relationships which may be considered as potential competing interests:Melaku Metto reports equipment and supplies were provided by Bahir Dar University. Melaku Metto reports a relationship with Injibara University that includes: employment. There is no competing body for the current work that could conflict If there are other authors, they declare that they have no known competing financial interests or personal relationships that could have appeared to influence the work reported in this paper.

Acknowledgments

Bahir Dar University's College of Sciences is acknowledged by the authors for providing access to laboratory resources. Sida (the Swedish International Development Cooperation Agency) through ISP (the International Science Programme, Uppsala University) is acknowledged for financial support.

Appendix A. Supplementary data

Supplementary data to this article can be found online at https://doi.org/10.1016/j.heliyon.2024.e38794.

References

[1] L. Rajith, K.G. Kumar, Electroanalysis of trimethoprim on metalloporphyrin incorporated glassy carbon electrode, Drug Test. Anal. 2 (9) (2010) 436–441.
[2] J.M. Ho, D.N. Juurlink, Considerations when prescribing trimethoprim-sulfamethoxazole, CMAJ (Can. Med. Assoc. J.) 183 (16) (2011) 1851–1858.
[3] Khushboo Gupta, Pranjul Shrivastava, Development and validation of UV spectrophotometric method for trimethoprim in pure and marketed formulation, Int. J. Health Sci. 6 (S2) (2022) 10829–10839.
[4] Yunhua He, Jiuru Lu, Mei Liu, Jianxiu Du, Molecular imprinting-chemiluminescence determination of trimethoprim using trimethoprim-imprinted polymer as recognition material, Analyst 130 (7) (2005) 1032–1037.
[5] Maria Feitosa, Anderson Santos, Ademar Wong, Robson Rocha, Fernando Moraes, Voltammetric determination of trimethoprim using a glassy carbon electrode modified with printex(6L) carbon and gold nanoparticles, Analytica 4 (2023) 159–169.
[6] Muhammad Aslam, Shahzad Ali, Mahmood Ahmed, Muhammad Javed, Afsah Iftikhar, Yousaf Abbas, Aamir Sohail, Mehvish Abdul-Rehman, Khansa Habibullah, Development and validation of RP-HPLC method for quantitative analysis of sulfamethoxazole and trimethoprim in liquid suspension: a comparative study with compendial method, Scientific Inquiry and Review 7 (2023) 19–34.
[7] Xizhuang Yue, Zaiyu Li, Shuang Zhao, A new electrochemical sensor for simultaneous detection of sulfamethoxazole and trimethoprim antibiotics based on graphene and ZnO nanorods modified glassy carbon electrode, Microchem. J. 159 (2020) 105440.
[8] Maria H.A. Feitosa, Anderson M. Santos, Ademar Wong, Robson S. Rocha, Fernando C. Moraes, Voltammetric determination of trimethoprim using a glassy carbon electrode modified with printex(6L) carbon and gold nanoparticles, Analytica 4 (2) (2023) 159–169.
[9] P.B. Deroco, R.C. Rocha-Filho, O. Fatibello-Filho, A new and simple method for the simultaneous determination of amoxicillin and nimesulide using carbon black within a dihexadecylphosphate film as the electrochemical sensor, Talanta 179 (2018) 115–123.
[10] Saeid Jafari, Mohammad Dehghani, Navid Nasirizadeh, Mohammad Hadi Baghersad, Mostafa Azimzadeh, Label-free electrochemical detection of Cloxacillin antibiotic in milk samples based on molecularly imprinted polymer and graphene oxide-gold nanocomposite, Measurement 145 (2019) 22–29.
[11] Adane Kassa, Atakilt Abebe, Meareg Amare, Synthesis, characterization, and electropolymerization of a novel Cu(II) complex based on 1,10-phenanthroline for electrochemical determination of amoxicillin in pharmaceutical tablet formulations, Electrochim. Acta 384 (2021) 138402.
[12] Adane Kassa, Meareg Amare, Electrochemical determination of paracetamol, rutin, and sulfonamide in pharmaceutical formulations by using glassy carbon electrode – a Review, Cogent Chemistry 5 (1) (2019) 1681607.
[13] Meareg Amare, Electrochemical characterization of iron (III) doped zeolite-graphite composite modified glassy carbon electrode and its application for AdsASSWV determination of uric acid in human urine, International Journal of Analytical Chemistry 2019 (2019) 6428072.
[14] Ersin Demir, A simple and sensitive square wave stripping pathway for the analysis of desmedipham herbicide by modified carbon paste electrode based on hematite (α-Fe2O3 nanoparticles), Electroanalysis 31 (8) (2019) 1545–1553.
[15] Ademar Wong, Anderson M. Santos, Camila A. Proença, Thaísa A. Baldo, Maria HA. Feitosa, Fernando C. Moraes, Maria DPT. Sotomayor, Voltammetric determination of 3-methylmorphine using glassy carbon electrode modified with rGO and bismuth film, Biosensors 12 (10) (2022) 860.
[16] Emre B. Boz, Marcell Fritz, Antoni forner-cuenca, electropolymerized poly(3,4-ethylenedioxythiophene) coatings on porous carbon electrodes for electrochemical separation of metals, Adv. Mater. Interfac. 10 (9) (2023) 2202497.
[17] Meareg Amare, Shimelis Admassie, Potentiodynamic fabrication, and characterization of poly(4-amino-3-hydroxynaphthalene sulfonic acid) modified glassy carbon electrode, J. Mater. Res. Technol. 9 (5) (2020) 11484–11496.
[18] Yiliyasi Baikeli, Xamxikamar Mamat, Mailidan Wumaer, Muhebaiti Muhetaer, Haji Akbar Aisa, Guangzhi Hu, Electrochemical determination of metronidazole using a glassy carbon electrode modified with nanoporous bimetallic carbon derived from a ZnCo-based metal-organic framework, J. Electrochem. Soc. 167 (11) (2020) 116513.
[19] Adane Kassa, Atakilt Abebe, Getinet Tamiru, Meareg Amare, Synthesis of a novel [diresorcinate-1,10-phenanthrolinecobalt(II)] complex, and potentiodynamic fabrication of poly(DHRPCo)/GCE for selective square wave voltammetric determination of procaine penicillin G in pharmaceutical and biological fluid samples, ChemistrySelect 7 (1) (2022) e202103458.
[20] Melaku Metto, Alemu Tesfaye, Minaleshewa Atlabachew, Atakilt Abebe, Synthesis, characterization, and electrochemical application of novel poly(Cu2P4BCl4) based glassy carbon electrodes for the determination of sulfamethoxazole in pharmaceutical serum and urine samples and Cow's milk, Microchem. J. 201 (2024) 110627.
[21] Yasemin Oztekin, Zafer Yazicigil, Preparation and characterization of a 1, 10-phenanthroline-modified glassy carbon electrode, Electrochim. Acta 54 (28) (2009) 7294–7298.
[22] Adane Kassa, Amare Benor, Getinet Tamiru, Atakilt Abebe, Characterization and application of a synthesized novel poly(chlorobis(1,10-phenanthroline) resorcinolcobalt(II) chloride)-modified glassy carbon electrode for selective voltammetric determination of cefadroxil in pharmaceutical formulations, human urine, and blood serum samples, ACS Omega 8 (2023).
[23] Joshua M. Sila, Peterson M. Guto, Immaculate N. Michira, Francis B. Mwaura, Edward K. Muge, Electrochemical determination of penicillin G in cow milk and pharmaceuticals in SDS/acetate buffer, Int. J. Electrochem. Sci. 16 (4) (2021) 210444.
[24] Yosef Bayeh, Atakilt Abebe, Madhu Nayathuparambil, Wolfgang Linert, Synthesis, Characterization and Antimicrobial Activities of New Mixed Ligand Complexes of Copper(II) with 1,10-Phenanthroline and Thymine, 2019.
[25] M. Amare, S. Aklog, Electrochemical determination of caffeine content in Ethiopian coffee samples using lignin modified glassy carbon electrode, J Anal Methods Chem 2017 (2017) 3979068.
[26] Hua Zhu, Li Yang, Yuqiao Song, Guangjin Zhao, Wenlong Wu, Shoubin Zhou, Dihua Wang, Wei Xiao, Effects of cyclic voltammetric scan rates, scan time, temperatures and carbon addition on sulphation of Pb disc electrodes in aqueous H2SO4, Mater. Technol. 35 (3) (2020) 135–140.
[27] Ibrahim Hudai Tasdemir, Abdulilah Ece, Esma Kilic, Experimental and theoretical study on the electrochemical behavior of zofenopril and its voltammetric determination, Curr. Pharmaceut. Anal. 8 (4) (2012) 339–348.
[28] J. Lang, W. Wang, Y. Zhou, D. Guo, R. Shi, N. Zhou, Electrochemical behavior and direct quantitative determination of paclitaxel, Front. Chem. 10 (2022) 834154.
[29] Tesfu Hailu, Merid Tessema, Yaw-Kuen Li, Electrochemical Determination of Chloramphenicol in Milk and Eye-Drop Using Easily Activated Screen Printed Carbon Electrodes, 2021.
[30] A. Abebe, T. Hailemariam, Synthesis and assessment of antibacterial activities of ruthenium(III) mixed ligand complexes containing 1,10-phenanthroline and guanide, Bioinorg Chem Appl 2016 (2016) 3607924.
[31] B Kaufman George, Inorganic chemistry: principles of structure and reactivity, (huheey, james e.; keiter, ellen a.; keiter, richard l.), ACS Publications, 1993.
[32] J Bard Allen, Larry R. Faulkner, Fundamentals and applications, Electrochemical methods 2 (482) (2001) 580–632.
[33] Peter Atkins, Julio De Paula, Elements of Physical Chemistry, Oxford University Press, USA, 2013.
[34] Azza A. Shoukry, Complex formation reactions of promethazine copper (II) and various biologically relevant ligands. Synthesis, equilibrium constants, spectroscopic characterization, and biological activity, J. Solut. Chem. 40 (2011) 1796–1818.
[35] Getasil Chanie, Adane Kassa, Getinet Tamiru Tigineh, Atakilt Abebe, Selective square wave voltammetric determination of tinidazole in pharmaceutical formulations, and human urine samples using poly(bis(2,2′-bipyridine)diresorcinolateruthenium(III) chloride) modified glassy carbon electrode, Sensing and Bio-Sensing Research 43 (2024) 100607.
[36] Adane Kassa, Meareg Amare, Amare Benor, Getinet Tamiru, Yonas Yohannes, Molla Tefera, Atakilt Abebe, Potentiodynamic poly(resorcinol)-modified glassy carbon electrode as a voltammetric sensor for determining cephalexin and cefadroxil simultaneously in pharmaceutical formulation and biological fluid samples, ACS Omega 7 (2022).
[37] Adane Kassa, Amare Benor, Getinet Tamiru Tigineh, Atakilt Abebe, Characterization and application of a synthesized novel poly(chlorobis(1,10-phenanthroline)resorcinolcobalt(II) chloride)-modified glassy carbon electrode for selective voltammetric determination of cefadroxil in pharmaceutical formulations, human urine, and blood serum samples, ACS Omega 8 (17) (2023) 15181–15192.

[38] Eva Sramkova, Tomas Bystron, Karel Bouzek, Quantification of electrocatalytic activity of glassy carbon electrode, Electrochim. Acta 379 (2021) 138177.
[39] Mandana Amiri, Hamideh Imanzadeh, Yasaman Sefid-Sefidehkhan, An overview on electrochemical sensors based on nanomaterials for the determination of drugs of abuse, Curr. Drug Deliv. 18 (2) (2021) 162–183.
[40] Arafat Toghan, Abo-Bakr Ahmed, Rageh Hm, Mohamed Abd-Elsabour, A novel electrochemical sensor for determination of salbutamol based on graphene oxide/poly (O-nitrobenzoic acid) modified glassy carbon electrode and its analytical application, in: Pharmaceutical Formulation and Human Urine, 2019.
[41] Mulu Gashu, Belete Asefa Aragaw, Molla Tefera, Voltammetric determination of oxytetracycline in milk and pharmaceuticals samples using polyurea modified glassy carbon electrode, J. Food Compos. Anal. 117 (2023) 105128.
[42] S.N. Prashanth, K.C. Ramesh, J. Seetharamappa, Electrochemical oxidation of an immunosuppressant, mycophenolate mofetil, and its assay in pharmaceutical formulations, International Journal of Electrochemistry (2011) 2011.
[43] Adane Kassa, Meareg Amare, Poly(4-amino-3-hydroxynaphthalene-1-sulfonic acid) modified glassy carbon electrode for square wave voltammetric determination of amoxicillin in four tablet brands, BMC Chemistry 15 (2021).
[44] Ameha Debalkie, Adane Kassa, Atakilt Abebe, Tihitinna Asmalash, Yonas Yohannes, Meareg Amare, Synthesis of a novel diaquabis(1,10-phenanthroline)copper (II)chloride complex and its voltammetric application for detection of amoxicillin in pharmaceutical and biological samples, Heliyon 8 (2022) e11199.
[45] Adane Kassa, Getinet Tamiru Tigineh, Atakilt Abebe, Electrochemical determination of chloroquine phosphate in real samples using a diresorcinate-1,10-phenanthrolinecobalt(II)-Modified glassy carbon electrode, ChemistryOpen 12 (3) (2023) e202300004.
[46] Elham Mirmomtaz, Asghar Ensafi Ali, Hassan Karimi-Maleh, Electrocatalytic determination of 6-tioguanine at ap-aminophenol modified carbon paste electrode, Electroanalysis: An International Journal Devoted to Fundamental and Practical Aspects of Electroanalysis 20 (18) (2008) 1973–1979.
[47] Allen J. Bard, Larry R. Faulkner, Henry S. White, Electrochemical Methods: Fundamentals and Applications, John Wiley & Sons, 2022.
[48] Adane Kassa, Atakilt Abebe, Getinet Tamiru, Meareg Amare, Synthesis of a novel [diresorcinate-1, 10-phenanthrolinecobalt (II)] complex, and potentiodynamic fabrication of poly (DHRPCo)/GCE for selective square wave voltammetric determination of procaine penicillin G in pharmaceutical and biological fluid samples, ChemistrySelect 7 (1) (2022) e202103458.
[49] M.H. Pournaghi-Azar, H. Razmi-Nerbin, Electrocatalytic characteristics of ascorbic acid oxidation at nickel plated aluminum electrodes modified with nickel pentacyanonitrosylferrate films, J. Electroanal. Chem. 488 (1) (2000) 17–24.
[50] Elham Mirmomtaz, Asghar Ensafi Ali, Hassan Karimi-Maleh, Electrocatalytic determination of 6-tioguanine at a p-aminophenol modified carbon paste electrode, Electroanalysis 20 (18) (2008) 1973–1979.
[51] Qicheng Qiao, Seema Singh, Shang-Lien Lo, Jierong Jin, Yong Chang Yu, Lizhang Wang, Effect of current density and pH on the electrochemically generated active chloro species for the rapid mineralization of p-substituted phenol, Chemosphere 275 (2021) 129848.
[52] Neeraj Kumar, Rosy, Rajendra Goyal, Gold-palladium nanoparticles aided electrochemically reduced graphene oxide sensor for the simultaneous estimation of lomefloxacin and amoxicillin, Sensor. Actuator. B Chem. 243 (2016).
[53] Aleksandra Pollap, Paweł Knihnicki, Piotr Kuśtrowski, Joanna Kozak, Monika Gołda-Cępa, Andrzej Kotarba, Jolanta Kochana, Sensitive voltammetric amoxicillin sensor based on TiO2 sol modified by CMK-3-type mesoporous carbon and gold nanoparticles, Electroanalysis 30 (10) (2018) 2386–2396.
[54] P. Daneshgar, P. Norouzi, M.R. Ganjali, A. Ordikhani-Seyedlar, H. Eshraghi, A dysprosium nanowire modified carbon paste electrode for determination of levodopa using fast Fourier transformation square-wave voltammetry method, Colloids Surf. B Biointerfaces 68 (1) (2009) 27–32.
[55] R.R. Sawkar, M.M. Shanbhag, S.M. Tuwar, R.S. Veerapur, N.P. Shetti, Glucose incorporated graphite matrix for electroanalysis of trimethoprim, Biosensors 12 (10) (2022).
[56] Peng Liu, Ruiying Zhang, Liyan Zheng, Qiue Cao, An electrochemical sensor for trimethoprim based on a magnetic molecularly imprinted carbon paste electrode, Chemosensors 11 (6) (2023) 339.
[57] Thais T. Guaraldo, Lorena A. Goulart, Fernando C. Moraes, Marcos RV. Lanza, Carbon black nanospheres modified with Cu (II)-phthalocyanine for electrochemical determination of Trimethoprim antibiotic, Appl. Surf. Sci. 470 (2019) 555–564.